Reactive $Ce_{0.8}RE_{0.2}O_{1.9}$ (RE = La, Nd, Sm, Gd, Dy, Y, Ho, Er, and Yb) Powders via Carbonate Coprecipitation. 1. Synthesis and Characterization

Ji-Guang Li,* Takayasu Ikegami, Toshiyuki Mori, and Toshiaki Wada

National Institute for Research in Inorganic Materials,† Namiki 1-1, Tsukuba, Ibaraki 305-0044, Japan

Received February 21, 2001. Revised Manuscript Received June 5, 2001

Nanocrystalline powders of ceria doped with 20 at. % of various rare-earth cations ($Ce_{0.8}RE_{0.2}O_{1.9}$, RE = La, Nd, Sm, Gd, Dy, Y, Ho, Er, and Yb) have been synthesized via coprecipitation using ammonium carbonate as the precipitant. The precursors and the resultant oxide powders were characterized by chemical analysis, differential thermal analysis/thermogravimetry (DTA/TG), X-ray diffractometry (XRD), and high-resolution scanning electron microscopy (HRSEM). The radius of RE^{3+} cations was found to have appreciable effects on chemical composition, thermal behavior, and particle morphology of the precursors and crystallite growth of the resultant oxide powders. The precursors obtained in this work possess a general formula of $(NH_4)_xCeRE_{0.25}(CO_3)_{1.875+x/2}\cdot yH_2O$ ($x = 1$ and $y = 1$ for RE = La, Nd, and Sm; while $x = 0.25$ and $y = 2$ for the rest), which decompose into oxides via oxycarbonate intermediates up to ≈410 °C upon heating. The precursors doped with RE^{3+} cations smaller than Sm^{3+} mainly consist of discrete primary particles of spherical shape, while those with larger cations (La^{3+}, Nd^{3+}, and Sm^{3+}) are mainly composed of secondary agglomerates of fibrous primary particles. The fluorite-structured $Ce_{0.8}RE_{0.2}O_{1.9}$ solid solutions are formed during calcination without any second phase detected with XRD, and the lattice parameters increase almost linearly with increasing ionic radius of the dopant. The coarsening rate of $Ce_{0.8}RE_{0.2}O_{1.9}$ crystallites during calcination varies with the radius of RE^{3+} cations, being highest for $Ce_{0.8}Sm_{0.2}O_{1.9}$ while lowest for $Ce_{0.8}La_{0.2}O_{1.9}$.

Introduction

Ceria can be doped with various rare-earth (RE) elements to form fluorite-structured solid solutions with an oxygen vacancies concentration depending upon the doping level. Rare-earth-doped ceria have been considered promising materials as oxygen-ion conducting electrolytes or electrodes for solid oxide fuel cells (SOFCs),[1−3] oxygen pumps,[1,4] and oxygen sensors.[1,5] The electrical conductivity of rare-earth-doped ceria was reported to increase with increasing doping level up to ≈10 mol % RE_2O_3[3] and after which decrease due to defect ordering, vacancy clustering, or electrostatic interaction.[1]

Rare-earth-doped ceria powders are typically produced via solid-state reaction starting from individual component oxides and/or carbonates, which requires repeated intermittent mechanical mixing and extensive heat treatment at high temperatures (such as 1300 °C for 10 h).[2−4,6] The resultant powders are usually characterized by large crystallite size, low surface area, and poor reactivity. These powders have to be densified by lengthy heating at temperatures as high as ≈1700−1800 °C to achieve the desired chemical homogeneity and density for applications as solid electrolytes.[2−4,6−8] Another disadvantage of the solid-state reaction method is the contamination during repeated mechanical mixing. It was found that the impurities form a liquid phase during high-temperature sintering, which subsequently becomes a highly resistive glassy phase along grain boundaries during the cooling period, severely blocking electrical conduction.[9−11]

Several kinds of wet-chemical methods[12−18] have been developed and successfully used for low-temperature synthesis of doped-ceria materials, and the resultant powders generally show finer crystallite/particle size and better reactivity than those via solid-state reaction. However, the sinterability has not been high enough. For example, oxalate coprecipitation, which has been

* To whom correspondence should be addressed: Sintered Materials Research Group, Advanced Materials Laboratory, National Institute for Materials Science, Namiki 1−1, Tsukuba, Ibaraki 305-0044, Japan. Fax: +81-298-52-7449. Tel.: +81-298-51-3354 (ext. 2247). E-mail: LI.Jiguang@nims.go.jp.

† Present name: Advanced Materials Laboratory, National Institute for Materials Science.

(1) Etsell, T. H.; Flengas, S. N. *Chem. Rev.* **1970**, *70*, 339.
(2) Kudo, T.; Obayashi, H. *J. Electrochem. Soc.* **1975**, *122*, 142.
(3) Dirstine, R. T.; Blumenthal, R. N.; Kuech, T. F. *J. Electrochem. Soc.* **1979**, *126*, 264.
(4) Subbarao, E. C.; Maiti, H. S. *Solid State Ionics* **1984**, *11*, 317.
(5) Steele, B. C. H. *Solid State Ionics* **1984**, *12*, 391.
(6) Eguchi, K.; Setoguchi, T.; Inoue, T.; Arai, H. *Solid State Ionics* **1992**, *52*, 165.
(7) Yahiro, H.; Eguchi, K.; Arai, H. *Solid State Ionics* **1989**, *36*, 71.
(8) Balazs, G. B.; Glass, R. S. *Solid State Ionics* **1995**, *76*, 155.
(9) Gerhardt, R.; Nowick, A. S. *J. Am. Ceram. Soc.* **1986**, *69*, 641.
(10) Gerhardt, R. Nowick, A. S.; Mochel, M. E.; Dumler, I. *J. Am. Ceram. Soc.* **1986**, *69*, 647.
(11) Aoki, M.; Chiang, Y. M.; Kosacki, I.; Lee, L. J. R.; Tuller, H.; Liu, Y. *J. Am. Ceram. Soc.* **1996**, *79*, 1169.

10.1021/cm010148x CCC: $20.00
Published on Web 08/23/2001

frequently used during recent years for powder synthesis, usually generates irregular-shaped and micrometer-sized particles, necessitating a typical sintering temperature of 1400−1600 °C to reach ≈99% of the theoretical even after using lengthy ball-milling to reduce particle size.[13,14,19] Sol−gel processing has been widely used for preparing various ceramic materials in various forms. This method, unfortunately, seems not so effective for producing reactive ceria-based oxides. Hung et al.[15] showed that the $Ce_{0.9}Gd_{0.1}O_{1.95}$ powder produced via sol−gel of nitrates can reach ≈99% of the theoretical only by sintering at a high temperature of ≈1600 °C. Rahaman and Zhou[17] have used a hydrothermal method to prepare ceria powders doped with various aliovalent cations, and well-dispersed powders, which can be sintered to be almost fully dense at a low temperature of ≈1300 °C, were obtained up to a doping level of 6 at. %. At a higher doping level of 20 at. %, however, the powders become severely agglomerated, and a much higher sintering temperature of 1450−1700 °C is required to reach ≈96−100% of the theoretical.[18,20] To the best of our knowledge, there has been no report concerning the sintering of $Ce_{0.8}RE_{0.2}O_{1.9}$ (hereafter referred to as 20REDC for convenience) solid-solution powders to >99% of the theoretical at temperatures below 1400 °C. Therefore, it is still highly desirable to develop new synthetic routes for producing highly reactive powders to lower the densification temperature. Lowering the densification temperature of 20REDC materials is meaningful for SOFCs applications, considering that it will allow the saving of energy, the use of conventional sintering furnaces without expensive heating elements, better mechanical properties of the electrolyte, and cofiring with other SOFCs components. Besides, even if the powder is contaminated during processing, the impurities may not form continuous resistive films along grain boundaries at low sintering temperatures, beneficial to electrical conductivity.

Coprecipitation is a relatively convenient method among wet-chemical methods for powder synthesis, and it is well-recognized that the characteristics and sinterability of the resultant oxide powders strongly depend on the type of starting salts and precipitant as well as synthesis conditions. Our previous work[21,22] developed a carbonate coprecipitation method to prepare reactive mixed oxides. The main advantage of carbonate coprecipitation over other synthetic methods, such as hydroxide coprecipitation and sol−gel, is that the precursors show much less agglomeration after drying and the resultant oxides exhibit good dispersion and excellent sinterability. In this work, we have used this carbonate coprecipitation method to prepare 20REDC (RE = La, Nd, Sm, Gd, Dy, Y, Ho, Er, and Yb) solid solutions. In the following sections, we describe the synthesis and characterization of the 20REDC materials.

Experimental Section

Powder Synthesis. Precursor powders were produced via coprecipitation using ammonium carbonate ($(NH_4)_2CO_3$, ultrahigh purity) as precipitant. The starting salts are rare-earth nitrate hexahydrates ($RE(NO_3)_3{\cdot}6H_2O$, RE = Ce, La, Nd, Sm, Gd, Dy, Y, Ho, Er, and Yb) with a purity of 99.99% and up. All the chemicals were purchased from Kanto Chemical Co., Inc., Tokyo, Japan, and were used as received without further purification.

The stock solution of starting salts was made by dissolving cerium nitrate hexahydrate and the corresponding dopant salt in distilled water. To ensure that Ce^{3+} and RE^{3+} cations would be mixed at the stoichiometric molar ratio of 4:1, cation contents of the mixed solution were assayed by the inductively coupled plasma (ICP) spectrophotometric technique and further adjusted. The final concentration of each stock solution was 0.15 M for Ce^{3+}. An aqueous solution of ammonium carbonate in distilled water with a concentration of 1.5 M was used as the precipitant.

Precipitation was performed on a hot plate equipped with a temperature controller and a magnetic stirrer. Typically, 300 mL of the mixed salt solution was dripped at a speed of 5 mL/min from a buret into 300 mL of the precipitant solution contained in a beaker kept at 70 °C under mild stirring. The resultant suspension was homogenized for 1 h after the completion of precipitation and was filtered using a suction filter. The precipitate was washed four times with distilled water and finally with anhydrous alcohol (except those for chemical analysis) before drying at room temperature under flowing nitrogen gas (200 mL/min) over 24 h. The dried precursor was then lightly crushed with a zirconia mortar and pestle and calcined in a tube furnace under flowing oxygen gas (50 mL/min) at various temperatures for 2 h.

Powder Characterization. Composition of the precursor was determined by chemical analysis. Cation contents were determined by the ICP spectrophotometric method with an accuracy of 0.01 wt %; carbon content was assayed on a simultaneous carbon/sulfur determinator with a detection limit of 0.01 wt % (Model CS-444LS, LECO, St. Joseph, MI); NH_4^+ content was determined by the distillation−titrimetric method with an experimental error of ±0.1 wt %; NO_3^- content was analyzed by the spectrophotometric method on a Ubest-35 spectrophotometer (Japan Spectroscopic Co., Ltd., Tokyo, Japan) with a detection limit of 0.01 wt %.

Differential thermal analysis/thermogravimetry (DTA/TG) of the dried precursor was made on a TG-DTA analyzer (Model TAS-200, Rigaku, Tokyo, Japan) under a flowing air (200 mL/min) atmosphere with a heating rate of 10 °C/min. The sample crucible was platinum with a depth of 5 mm, and the reference material was alpha-alumina.

Phase identification was performed via X-ray diffractometry (XRD) on a Philips PW1800 X-ray diffractometer (Philips Research Laboratories, The Netherlands) operated at 40 kV/50 mA using nickel-filtered Cu Kα radiation in the range of $2\theta = 20°-100°$ with a scanning speed of 0.5° 2θ/min. Lattice parameters of the 20REDC solid solutions were determined by fitting the observed reflections with a least-squares refinement program. Crystallite sizes of the calcined powders were calculated by the X-ray line-broadening technique performed on the (422) diffraction[17] of ceria lattice using computer software (APD 1800, Philips Research Laboratories) from the Scherrer equation,

(12) Dragoo, A. L.; Domingues, L. P. *J. Am. Ceram. Soc.* **1982**, *65*, 253.
(13) Duran, P.; Moure, C.; Jurado, J. R. *J. Mater. Sci.* **1994**, *29*, 1940.
(14) Hertle, J. V.; Horita, T.; Kawada, T.; Sakai, N.; Yokokawa, H.; Dokiya, M. *Ceram. Int.* **1998**, *24*, 229.
(15) Huang, K.; Feng, M.; Goodenough, J. B. *J. Am. Ceram. Soc.* **1998**, *81*, 357.
(16) Chen, C. C.; Nasrallah, M. M.; Anderson, H. U. *J. Electrochem. Soc.* **1993**, *140*, 3555.
(17) Rahaman, M. N.; Zhou, Y. C. *J. Euro. Ceram. Soc.* **1995**, *15*, 939.
(18) Huang, W.; Shuk, P.; Greenblatt, M. *Chem. Mater.* **1997**, *9*, 2240.
(19) Higashi, K.; Sonoda, K.; Ono, H.; Sameshita, S.; Hirata, Y. *J. Mater. Res.* **1999**, *14*, 957.
(20) Yamashita, K.; Ramanujachary, K. V.; Greenblatt, M. *Solid State Ionics* **1995**, *81*, 53.
(21) Li, J. G.; Ikegami, T.; Lee, J. H.; Mori, T. *J. Mater. Res.* **2000**, *15*, 1514.
(22) Li, J. G.; Ikegami, T.; Lee, J. H.; Mori, T. *J. Am. Ceram. Soc.* **2000**, *11*, 2866.

$$D = 0.9\lambda/(\beta \cos \theta) \quad (1)$$

where D is the average crystallite size, λ is the wavelength of incident X-rays (0.154 06 nm), θ is the diffraction angle, and β is the corrected half-width given by

$$\beta^2 = \beta_m{}^2 - \beta_s{}^2 \quad (2)$$

where β_m is the measured half-width and β_s is the half-width of a standard CeO_2 sample with a known crystallite size of larger than 150 nm.

Particle morphology and agglomeration state of the synthesized powders were observed via high-resolution scanning electron microscopy (HRSEM) (Model S-5000, Hitachi, Tokyo, Japan). The sample was ultrasonically dispersed in ethanol, and the suspension was spread on the surface of a silicon plate. After the sample dried at room temperature, a thin layer of osmium was coated on the sample surface for conductivity before observation.

Results and Discussion

Chemical Composition of the Precursor. Composition of the precursor depends on the supporting anions present and the solubilities of metal cations in solution. The following equilibria were expected in the precipitant solution:

$$H_2O \leftrightarrows H^+ + OH^- \quad (3)$$

$$(NH_4)_2CO_3 \leftrightarrows 2NH_4{}^+ + CO_3{}^{2-} \quad (4)$$

$$NH_4{}^+ + OH^- \leftrightarrows NH_4OH \quad (5)$$

$$NH_4OH \leftrightarrows H_2O + NH_3(g) \quad (6)$$

$$H^+ + CO_3{}^{2-} \leftrightarrows HCO_3{}^- \quad (7)$$

$$H^+ + HCO_3{}^- \leftrightarrows H_2CO_3 \quad (8)$$

and

$$H_2CO_3 \leftrightarrows H_2O + CO_2(g) \quad (9)$$

On the other hand, lanthanide cations are known to undergo weak hydration and slight hydrolysis in water to form complex species,[23]

$$RE(H_2O)_n{}^{3+} + H_2O \leftrightarrows [RE(OH)(H_2O)_{n-1}]^{2+} + H_3O^+ \quad (10)$$

where n is the coordination number of RE^{3+} cations. The equilibrium shifts rightward with increasing atomic number of lanthanide elements, as would be expected from the contraction in ionic radii. It should be noted that yttrium does not belong to lanthanides, but Y^{3+} cations observe the "lanthanide contraction law" and exhibit chemical properties close to those of Ho^{3+}.[24] During precipitation, the complexes formed in eq 10 are reacted with carbonate anions and other supporting ionic species generated through eqs 3−9 to form precipitates, and the final composition should ensure that

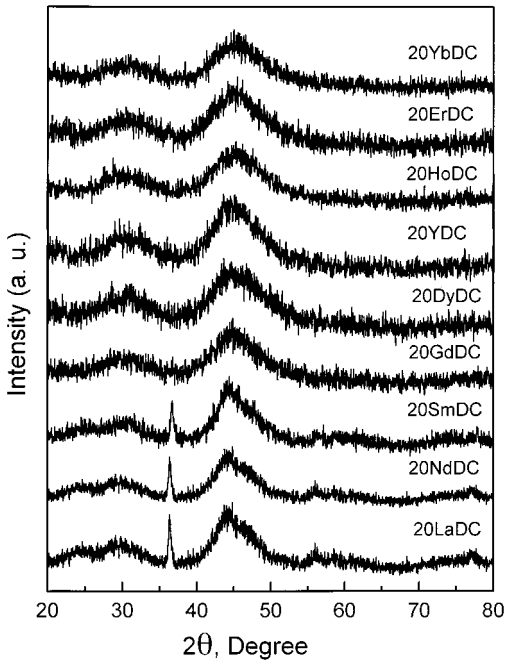

Figure 1. XRD patterns of the as-dried 20REDC precursors.

Ce^{3+} and RE^{3+} cations have the lowest solubilities in solution under the present precipitation conditions.

Figure 1 shows XRD patterns of the as-dried 20REDC precursors. All the powders show low crystallinity, making it difficult to perform phase identification and composition determination via the XRD method. The ionic radius of dopant seems to affect properties of the precursor. Considering 8-fold coordination in the fluorite structure, the ionic radius of dopant[25] (in nanometer) increases in the following order: Yb^{3+} (0.0985) < Er^{3+} (0.1004) < Ho^{3+} (0.1015) < Y^{3+} (0.1019) < Dy^{3+} (0.1027) < Gd^{3+} (0.1053) < Sm^{3+} (0.1079) < Nd^{3+} (0.1109) < La^{3+} (0.1160). Figure 1 clearly shows that the precursors doped with larger cations (La^{3+}, Nd^{3+}, and Sm^{3+}) have an additional peak at a diffraction angle of $2\theta \approx 36°$, while those doped with cations smaller than Sm^{3+} lack the diffraction.

Chemical analysis confirmed that the stoichiometry of starting salt solutions has been kept to the precursors after precipitation, and all the precursors have a stoichiometric molar ratio of Ce^{3+}:RE^{3+} = 4:1 within the accuracy of the analysis method (0.01 wt %). $NO_3{}^-$ is not a precipitating anion here and its content in the precursor is below the detection limit of 0.01 wt %. In accordance with the results of XRD analysis, chemical analysis revealed that the precursors assume two kinds of chemical formulas depending upon the ionic radius of the dopant:

$$(NH_4)CeRE_{0.25}(CO_3)_{2.375}\cdot H_2O \quad (RE = La, Nd, and Sm) \quad (11)$$

and

$$(NH_4)_{0.25}CeRE_{0.25}(CO_3)_{2.0}\cdot 2H_2O \quad (RE = Gd, Dy, Y, Ho, Er, and Yb) \quad (12)$$

where the coefficients of molecular water were calcu-

(23) Topp, N. E. *The Chemistry of Rare-Earth Elements*; Elsevier: Amsterdam, 1965.

(24) Sidgwick, N. V. *The Chemical Elements and Their Compounds*; Clarendon: Oxford, 1962.

(25) Shannon, R. D. *Acta Crystallogr.* **1976**, *A32*, 751.

lated from the weight contents of Ce or RE (determined by chemical analysis) in the precursors.

The ammonium rare-earth carbonate precursors obtained in this work can be viewed as the normal carbonates coordinated with NH_4^+ and additional CO_3^{2-} according to the stoichiometry of ammonium carbonate. Similar results were obtained from other material systems[21,26,27] when ammonium carbonate or ammonium bicarbonate in large excess was used as the precipitant. The precursors synthesized in this work show quite different chemical compositions from those via urea-based homogeneous precipitation[28−30] or homogeneous precipitation by thermal decomposition of trichloroacetates under carbon dioxide pressures,[31,32] though carbonate anions are similarly involved in the latter two systems. The urea-based homogeneous precipitation method usually generates basic carbonates of the general formula $RE(OH)CO_3 \cdot xH_2O$ under ambient pressure, while normal carbonates of various rare-earth elements have been produced through thermal decomposition of the corresponding trichloroacetates in solution. Obviously, the concentration of carbonate anions and the presence of high-concentration NH_4^+ cations have played important roles in determining chemical composition of the precursor.

The Results of DTA/TG Analysis. The thermal behavior of precursors has been investigated by DTA/TG analysis. Chemical composition was found to have substantial effects on thermal decomposition, and the results can be classified into two groups according to formulas (11) and (12). In each group, however, the precursors show nearly identical behaviors and no clear trend was observed concerning the effect of dopant size on the thermal decomposition process. Besides, for any precursor obtained in this work, the ultimate weight loss revealed by TG is within a narrow deviation of ±1.0% from that calculated from its chemical formula. We select here 20LaDC and 20GdDC as representatives for their corresponding groups and characterize their thermal decomposition processes.

Figure 2 shows DTA/TG curves of the 20LaDC and 20GdDC precursors. For both powders, no clear thermal events corresponding to crystallization processes were identified on the DTA curves. TG curves revealed that the decomposition of 20LaDC and 20GdDC precursors into oxides mainly occurred below ≈350 and ≈410 °C with final weight losses of ≈39.80 and ≈36.39%, respectively. These weight losses agree well with those calculated from the complete decomposition of $(NH_4)CeLa_{0.25}(CO_3)_{2.375} \cdot H_2O$ (39.76%) and $(NH_4)_{0.25}CeGd_{0.25}(CO_3)_{2.0} \cdot 2H_2O$ (36.04%), noticing that Ce^{3+} cations are

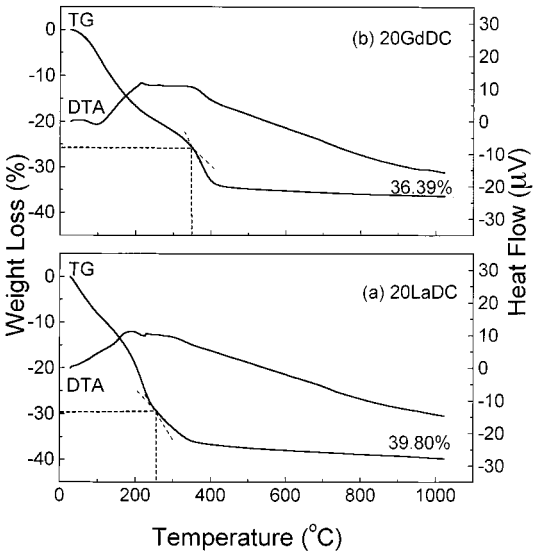

Figure 2. Simultaneous DTA/TG curves of the 20LaDC and 20GdDC precursors.

oxidized to Ce^{4+} during heating.[30] The thermal decomposition of both precursors proceeds through two stages, with the first one corresponding to the partial decomposition of the ammonium rare-earth carbonates into oxycarbonates[31,32] and the second one corresponding to the further decomposition of oxycarbonates into oxides. The decomposition process can be generally described as

$$(NH_4)_xCeRE_{0.25}(CO_3)_{1.875+x/2} \cdot nH_2O \rightarrow CeRE_{0.25}O_{0.875}(CO_3) \rightarrow CeRE_{0.25}O_{2.375} \quad (20REDC) \quad (13)$$

where $x = 1$ and $n = 1$ for RE = La, Nd, and Sm, while $x = 0.25$ and $n = 2$ for RE = Gd, Dy, Y, Ho, Er, and Yb. The calculated weight losses for the first stage decomposition of 20LaDC precursor (29.57%) and 20GdDC precursor (25.45%) are in good agreement with those revealed by TG analysis (≈29.3% at 255 °C for 20LaDC and ≈25.5% at 348 °C for 20GdDC), as indicated on the TG curves in Figure 2.

The Results of XRD Analysis. We have made a systematic study on the phase evolution of 20REDC precursors during calcination. Each precursor was calcined at the selected temperatures for 2 h under flowing oxygen gas and then subjected to XRD analysis after cooling to room temperature. It was found that all the powders, regardless of the ionic radius of the dopant, begin to crystallize at a minimum temperature of ≈300 °C from an amorphous phase at even lower temperatures. At 300 °C, the samples have already displayed almost all the characteristic reflections corresponding to the fluorite structure of CeO_2 (JCPDS: pattern 34-394). Above 300 °C, continued refinements in peak shapes and intensities were observed along with an increase in the calcination temperature, indicating crystallite growth. For any 20REDC material in this work, no other crystalline phases were detected along with the fluorite-structured solid solution at any calcination temperature above 300 °C, indicating high cation homogeneity in the precursor.

Figure 3 compares XRD patterns of the 20REDC powders calcined at 700 °C. The diffraction peaks gradually shift toward the high-angle side with decreasing ionic radius of the dopant, indicating a gradual

(26) Kato, S.; Iga, T.; Hatano, S.; Isawa, Y. *J. Ceram. Soc. Jpn.* **1976**, *84*, 215.
(27) Li, J. G.; Ikegami, T.; Lee, J. H.; Mori, T.; Yajima, Y. *J. Euro. Ceram. Soc.* **2001**, *21*, 139.
(28) Akinc, M.; Sordelet, D. J.; Munson, M. *Adv. Ceram. Mater.* **1988**, *3*, 211.
(29) Akinc, M.; Sordelet, D. J. *Adv. Ceram. Mater.* **1987**, *2*(*3A*), 232.
(30) Matijevic, E.; Hsu, W. P. *J. Colloid Interface Sci.* **1987**, *118*, 506.
(31) Head, E. L.; Holly, C. E., Jr. The Preparation and Thermal Decomposition of Some Rare Earth Carbonates. In *Rare Earth Research II*; Vorres, K. S., Ed.; Gordon and Breach: London, 1964.
(32) Head, E. L.; Holly, C. E., Jr. The Preparation and Thermal Decomposition of the Carbonates of Tb, Dy, Ho, Er, Tm, Yb, Lu, Y, and Sc. In *Rare Earth Research III*; Eyring, L., Ed.; Gordon and Breach: London, 1965.

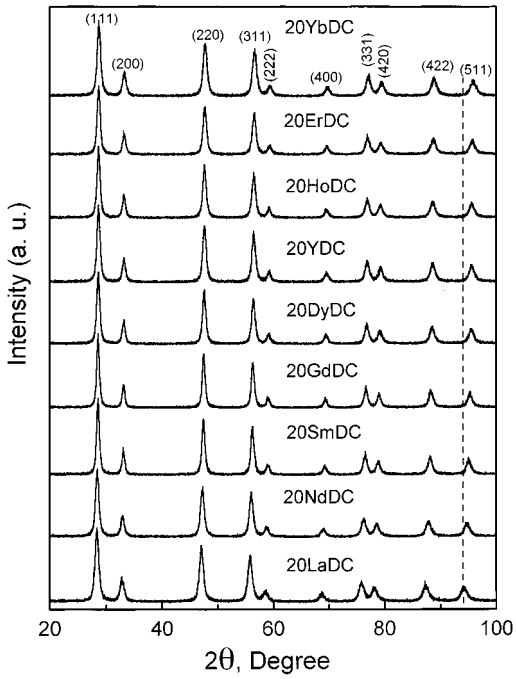

Figure 3. A comparison of the XRD patterns of 20REDC powders calcined at 700 °C for 2 h.

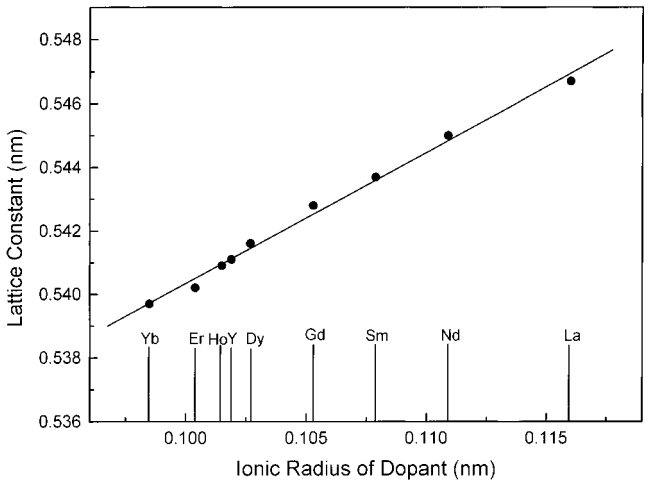

Figure 4. Lattice parameters of the 20REDC oxides calcined at 700 °C, as a function of the ionic radius of the dopant.

contraction in the unit cell. Figure 4 exhibits lattice parameters of the 20REDC solid solutions calcined at 700 °C, as a function of the ionic radius of dopant. The lattice parameters increase almost linearly with increasing ionic radius of the dopant and are in reasonable agreement with previously reported data.[1,2,4]

The evolution of crystallite size during calcination has been investigated for each 20REDC powder, and the results obtained from X-ray line-broadening of the (422) peak are summarized in Figure 5. It can be seen that the crystallite size of each sample shows an exponential dependence on the calcination temperature, indicating that crystallite growth is diffusion-related. The ionic radius of dopant has dramatic effects on the rate of crystallite coarsening. Though the crystallite sizes of 20REDC powders are very similar and fall in a very narrow range of ≈5.3−6.1 nm at 500 °C, the differences among them are gradually widened with increasing calcination temperature. Figure 6 presents the crystallite sizes of 20REDC powders calcined at 900 °C, as a function of the ionic radius of the dopant. It clearly shows that the rate of crystallite coarsening increases gradually with increasing ionic radius of the dopant from Yb to Sm and then decreases with a further increase in dopant size.

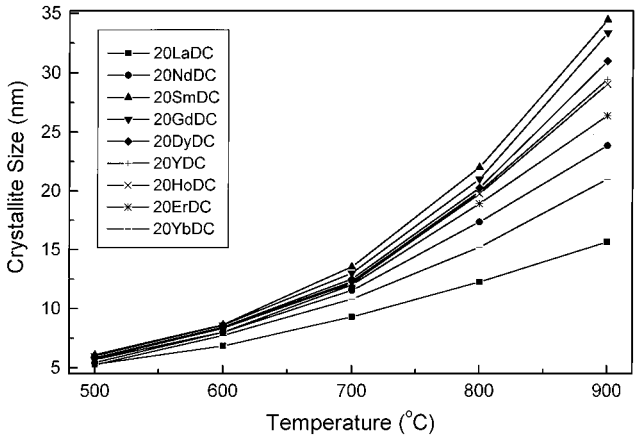

Figure 5. Crystallite size of the 20REDC powders, as a function of the calcination temperature.

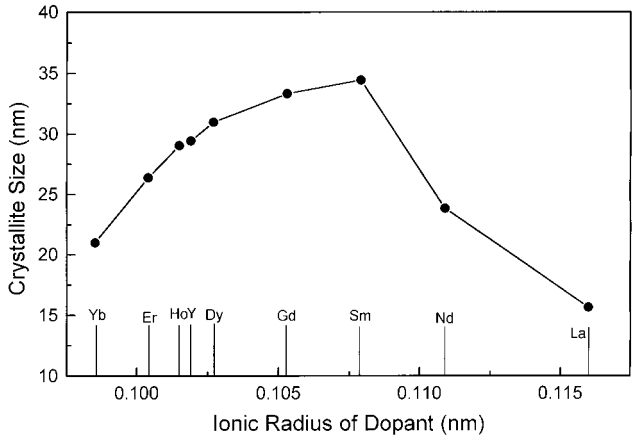

Figure 6. Crystallite size of the 20REDC powders calcined at 900 °C for 2 h, as a function of the ionic radius of the dopant.

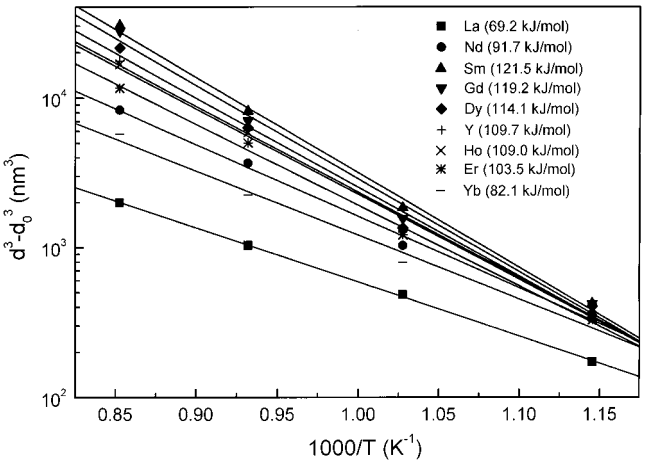

Figure 7. Crystallite growth versus reciprocal temperature according to the cubic law; dopants and activation energies indicated.

Crystallite growth is a process of mass transportation. Though oxygen diffusion has been recognized as the rate-controlling factor for many diffusion-related phenomena (such as sintering) in various oxide ceramic

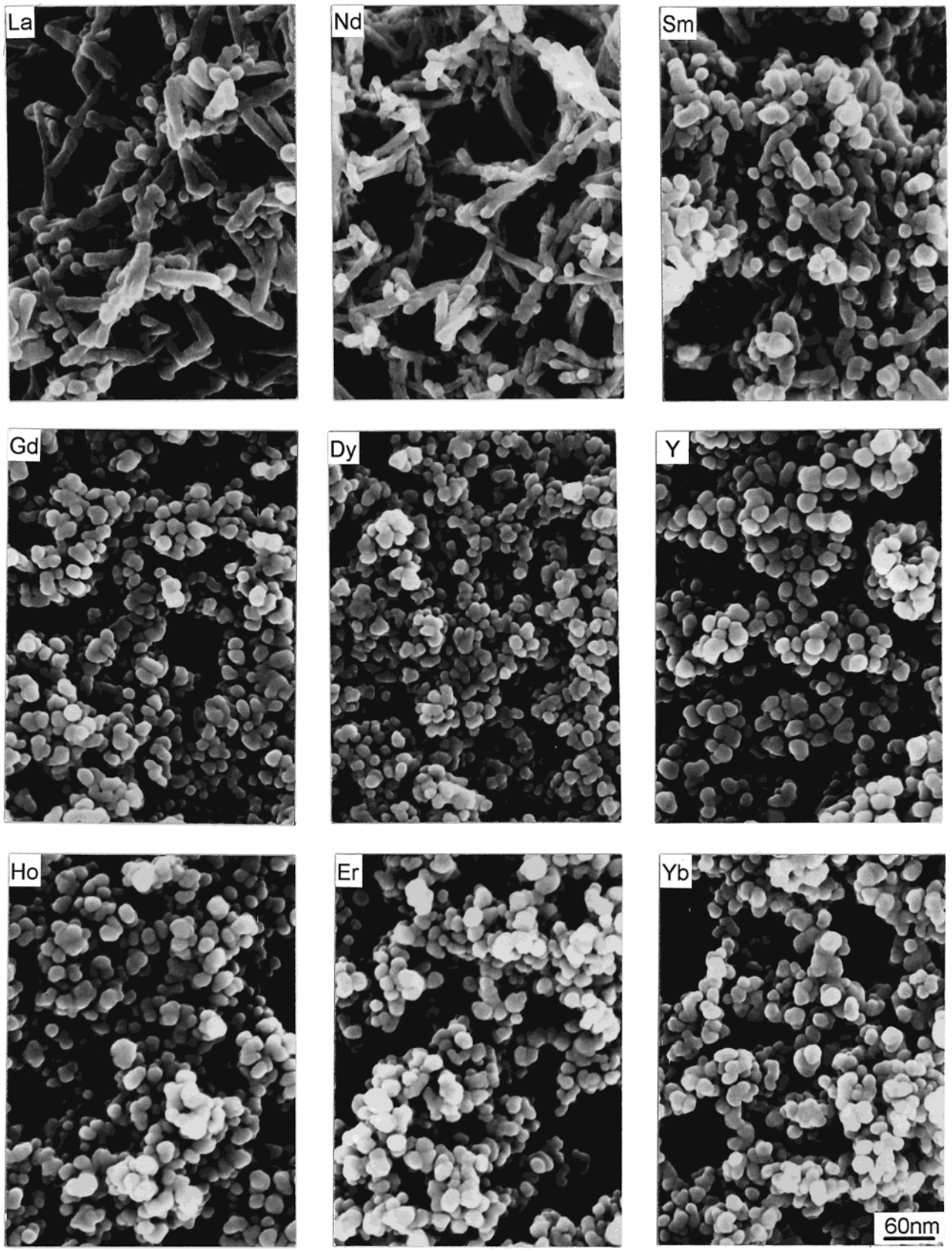

Figure 8. HRSEM micrographs showing particle morphologies of the 20REDC precursors. The corresponding dopants are indicated in the pictures, and the scale bar for 20YbDC is applicable to other materials.

materials, it is not the rate-controlling factor for the crystallite growth of 20REDC oxides since oxygen diffusion was reported to be several orders of magnitude faster than cation diffusion in fluorite-structured solid electrolytes.[1] The variation of crystallite growth rate with dopant size, therefore, cannot be simply rationalized in terms of the diffusivity of oxygen ions. It is concluded from Figures 5 and 6 that the diffusivity of

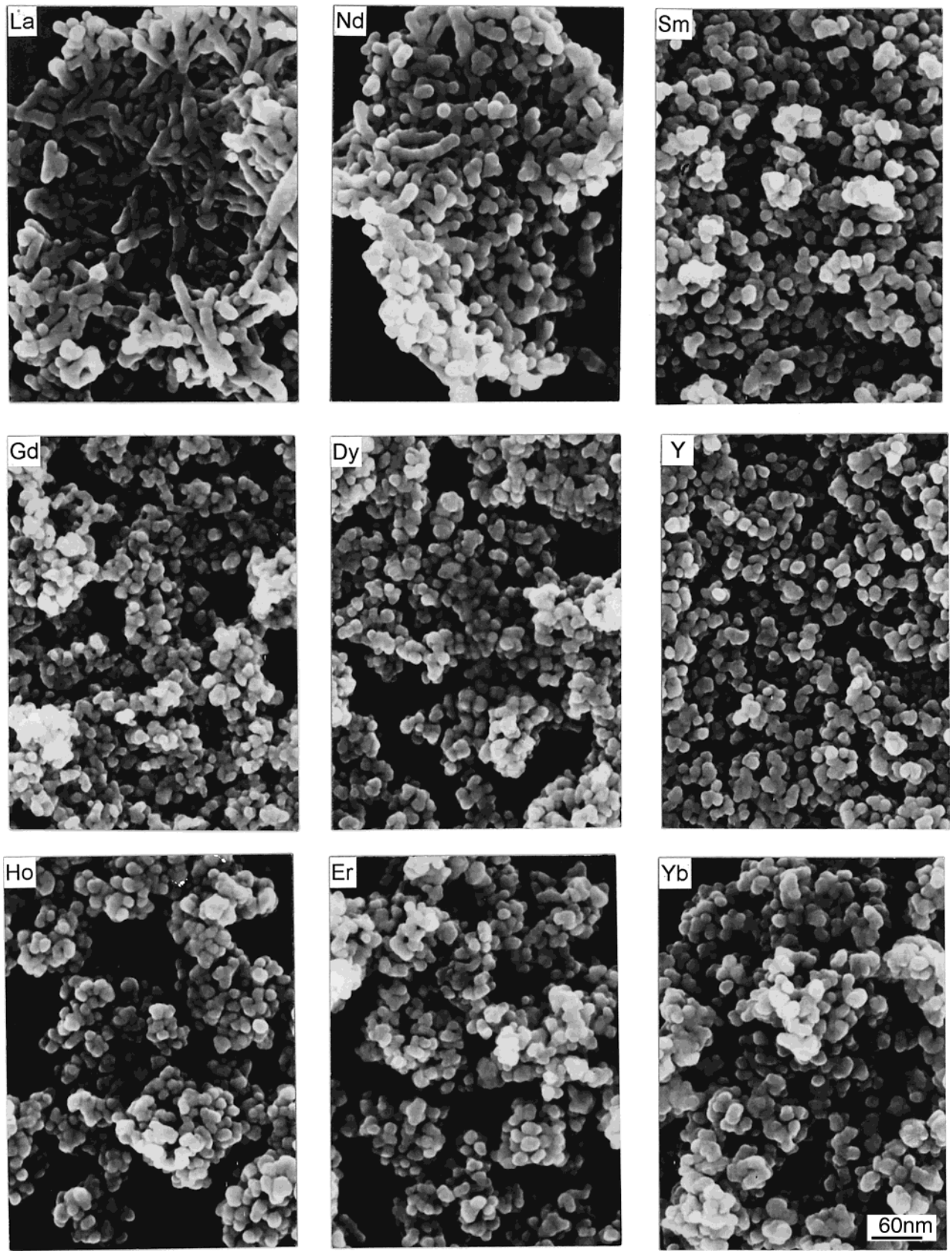

Figure 9. HRSEM micrographs showing particle morphologies of the 20REDC powders calcined at 700 °C for 2 h. The corresponding dopants are indicated in the pictures, and the scale bar for 20YbDC is applicable to other materials.

cations in 20REDC oxides strongly depends on the dopant size.

It is observed that the coarsening of 20REDC crystallites follows the "cubic law", as expressed below, which implies that surface and interface phenomena (such as grain-boundary potential and solute segregation at particle surfaces and grain boundaries due to space charge) may have played important roles in influ-

encing mass transportation and crystallite growth.[33−35]

$$d^3 - d_0^3 = A \exp(-Q/RT) \quad (14)$$

where d_0 and d are the average crystallite diameters at and above 500 °C, respectively. A is a pre-exponential constant, Q denotes the activation energy, R is the gas constant, and T is the absolute temperature. The crystallite growth during the rising period of calcination is neglected here due to its small contribution (<10%) to the total crystallite size. Figure 7 shows the temperature dependence of crystallite size on a log−log plot, with the activation energies indicated in the figure. It can be seen that the activation energy for crystallite growth varies with dopant size, and the material of a higher coarsening rate shows a higher activation energy. More research work is necessary to elaborate on the micromechanisms of crystallite coarsening.

Powder Morphology. We have observed morphologies of the precursors and the resultant oxide powders using HRSEM. Dopant size affects both the dispersion state and the shape of primary particles, and the results can also be categorized according to formulas (11) and (12). Though not shown here, low-magnification observation indicates that the primary particles of precursors doped with larger cations (La^{3+}, Nd^{3+}, and Sm^{3+}) mainly exist in the form of agglomerates sized ≈15 μm, while those of the precursors doped with smaller cations are in a discrete state. Figure 8 shows typical particle morphologies of 20REDC precursors under high magnification. The primary particles of 20LaDC and 20NdDC are fibrous and floc into porous secondary agglomerates. Decreasing dopant size tends to change the primary particles from fibrous to spherical shapes. Though the 20SmDC precursor still contains some elongated particles of lower aspect ratio, those doped with even smaller cations are only composed of uniformly sized primary particles of spherical shape and show good dispersion.

Figure 9 shows morphologies of the 20REDC powders calcined at 700 °C for 2 h. Like their precursors, the powders doped with cations smaller than Sm^{3+} are mainly composed of uniformly sized, spherical-shaped, discrete particles. Dopant size affects the agglomeration strength of primary particles in 20LaDC, 20NdDC, and 20SmDC precursors. The agglomerates in 20SmDC completely collapsed into discrete particles during calcination, while the pseudomorphs of agglomerates in 20LaDC and 20NdDC remained after calcination. Besides, most of the fibrous primary particles in 20NdDC are broken into rounded particles by calcination at 700 °C, while those in 20LaDC remain nearly unchanged under the identical calcination conditions.

The 20REDC powders calcined at 700 °C are highly reactive and can be sintered to be >99.5% dense at very low temperatures of ≈1100−1250 °C. Detailed studies on the densification behaviors of the 20REDC solid solutions will be reported in the following paper.

Conclusions

Nanocrystalline $Ce_{0.8}RE_{0.2}O_{1.9}$ (RE = La, Nd, Sm, Gd, Dy, Y, Ho, Er, and Yb) powders have been successfully synthesized via coprecipitation using ammonium carbonate as the precipitant. The radius of RE^{3+} cations was found to have appreciable effects on composition, thermal behavior, and particle morphology of the precursors and crystallite growth of the resultant oxide powders. The precursors obtained in this work are ammonium rare-earth carbonate hydrates, which decompose into oxides up to ≈410 °C via oxycarbonate intermediates. The precursors doped with RE^{3+} smaller than Sm^{3+} mainly consist of discrete primary particles of spherical shape, while those with larger cations (La^{3+}, Nd^{3+}, and Sm^{3+}) are mainly composed of secondary agglomerates of fibrous primary particles. The coarsening rate of $Ce_{0.8}RE_{0.2}O_{1.9}$ solid solutions during calcination varies with the radius of RE^{3+} cations, being highest for $Ce_{0.8}Sm_{0.2}O_{1.9}$ while lowest for $Ce_{0.8}La_{0.2}O_{1.9}$.

CM010148X

(33) Cahn, J. W. *Acta Metall.* **1962**, *10*, 789.
(34) Hillert, M. *Acta Metall.* **1965**, *13*, 227.
(35) Kingery, W. D.; Bowen, H. K.; Uhlmann, D. R. *Introduction to Ceramics*; John Wiley & Sons: New York, 1976.